Spin-orbit Torque in Structures with Magnetization-compensated MnGa/Co_2MnSi bilayer

Takuya Hara (原 拓也)[1], Kohey Jono (城野航平)[1], Michihiko Yamanouchi (山ノ内路彦)[1], and Tetsuya Uemura (植村哲也)[1]

[1]Graduate School of Information Science and Technology, Hokkaido University, Sapporo 060-0814, Japan

We have systematically investigated the spin-orbit torque (SOT) induced effective magnetic field in a structure consisting of a Ta heavy metal layer and an antiferromagnetically coupled MnGa/Co_2MnSi (CMS) bilayer around the magnetization compensation point by varying the CMS film thickness. The efficiency of SOT generation takes the maximum around the compensation point, and it is approximately 6 times as large compared with that in the devices with a MnGa single structure. The enhancement of SOT efficiency can be explained mainly by the reduction of saturation magnetic moment around the compensation point. Moreover, a significant enhancement of the effective spin Hall angle was observed around the compensation point because of the inversion of the magnetization configuration before and after the compensation point.

***Index Terms*—spin-orbit torque, synthetic antiferromagnetic structure, MnGa, Co_2MnSi**

I. Introduction

Magnetic random access memory (MRAM) utilizing the spin-orbit torque (SOT) induced magnetization switching has attracted much interest as a next-generation non-volatile memory featuring high-speed switching and high writing endurance [1]-[8]. The synthetic antiferromagnetic (SAF) structure, in which two or more thin ferromagnetic layers are antiferromagnetically coupled, is promising for a recording layer of SOT-MRAM because of low stray magnetic field and high thermal stability. Moreover, high SOT efficiency is also expected for the SAF structure due to low saturation magnetic moment because the efficiency of SOT generation is inversely proportional to the magnetization of the ferromagnetic layer [9].

A Mn_xGa_1 (MnGa)/Co_2MnSi (CMS) bilayer is one of the candidates for the above-mentioned ferromagnetic electrodes due to the following features. MnGa and CMS layers are antiferromagnetically coupled to each other [10], which results in forming the SAF structure. A MnGa exhibits relatively large perpendicular magnetic anisotropy (PMA) [11]-[13], and there have been several reports on MnGa-based perpendicular magnetic tunnel junctions (p-MTJs) [14]. SOT-induced magnetization switching in ultrathin MnGa structures [15]-[20] have also been reported. On the other hand, a CMS is theoretically predicted to show a half-metallic nature [21]-[23], and high TMR ratios have been experimentally demonstrated in CMS-based MTJs [24]-[28]. Thus, a p-MTJ with MnGa/CMS free layer is expected to exhibit high TMR ratio and high thermal stability.

Recently, we have reported the SOT magnetization switching with low switching current density in a MnGa/CMS bilayer compared to a MnGa single layer [29]. However, the magnetization was not compensated in the previous MnGa/CMS bilayer. To take full advantage of the SAF structure, the magnetization of the bilayer should be compensated. Although Li et al., realized magnetization compensation in a MnGa/CMS bilayer by changing the temperature, and reported the SOT switching characteristics [30], the effect of magnetization compensation on the SOT properties is still not fully understood. Given these backgrounds, the purpose of this study is to clarify the efficiency of SOT generation near the magnetization-compensation point in a MnGa/CMS bilayer structure with a Ta acting as the source of SOT. For this purpose, we systematically controlled the magnetization in MnGa/CMS bilayers by varying the CMS thicknesses (t_{CMS}) on the same substrate and investigated the t_{CMS}-dependence of SOT-induced effective magnetic field.

II. Experimental method

A layer structure consisting of (from the substrate side) MgO buffer (10)/$Ni_{1.1}Al_1$ (NiAl) buffer (5)/MnGa (2.5)/CMS (0–1.7)/Ta (5)/MgO cap (2) was grown on a (001) MgO single-crystalline substrate [Fig. 1(a)]. The numbers in parentheses are nominal thicknesses in nanometers. A 2.5-nm-thick MnGa was grown on a NiAl buffer layer by molecular-beam epitaxy at 200℃ and was annealed at 300℃. Then, a CMS wedged layer was grown by rf magnetron sputtering at room temperature and then was annealed at 400℃. The thickness of CMS was varied from 0 to 1.7 nm on the same substrate by using a sliding shutter to realize the magnetization compensation. Finally, a 5-nm thick Ta was deposited by dc sputtering at room temperature as an SOT spin source. The composition of MnGa was $Mn_{1.8}Ga_1$ from inductively coupled plasma (ICP) optical emission spectroscopy measurements. In order to investigate the influence of NiAl buffer on the SOT characteristics, a 2.5-nm-thick MnGa single layer without Ta was also grown. The structural and magnetic properties of MnGa/CMS bilayer were

Manuscript received November 1, 2021; revised December 27, 2021; accepted December 28, 2021. Date of publication **, 2021; date of current version **, 2021. Corresponding author: T. Uemura (e-mail: uemura@ist.hokudai.ac.jp). Color versions of one or more of the figures in this paper are available online at http://ieeexplore.ieee.org.

Digital Object Identifier (inserted by IEEE).

characterized by reflection high-energy electron diffraction (RHEED) observations and magneto-optical Kerr effect (MOKE) measurement. The layer structure was processed into Hall devices with a 5-μm-wide channel by photolithography and Ar ion milling. We measured the transverse resistance R_{yx} to investigate the SOT-induced effective magnetic field at room temperature. A schematic of the measurement setup with a definition of the Cartesian coordinate system is shown in Fig. 1(b).

III. Result and discussion

A. Structural and magnetic properties

Fig. 1(c) shows RHEED patterns of MnGa and CMS layers under the electron beam azimuth along MgO[100] direction. We observed clear streak patterns for MnGa and CMS, indicating the epitaxial growth of both MnGa and CMS. Moreover, we observed clear 11* superlattice lines of the CMS after 400˚C annealing, suggesting that the CMS film was $L2_1$-ordered.

Fig. 2(a) shows the polar MOKE signals of MnGa/CMS bilayer measured at room temperature for various t_{CMS} ranging from 0 to 1.55 nm as a function of $\mu_0 H_z$, where μ_0 is the permeability of vacuum and H_z is the out-of-plane magnetic field. Clear hysteresis loops reflecting the PMA of both MnGa and CMS were observed for $t_{CMS} \leq 1.15$ nm except for t_{CMS} = 0.45 nm. The amplitude of the hysteresis loops decreased and the coercive field increased as increasing t_{CMS} from 0 to 0.4 nm, indicating that the MnGa and CMS are antiferromagnetically coupled to each other. For $t_{CMS} > 0.55$ nm, the polarity of the hysteresis loops changed. This indicates that the magnetic moment of CMS becomes larger than that of MnGa, and the MnGa is magnetized antiparallel to the magnetic field. Thus, the magnetization compensation is realized at $t_{CMS} \approx 0.45$ nm. The coercive field decreased with increasing t_{CMS} from 0.55 nm to 1.55 nm because the influence of CMS favoring the in-plane magnetic anisotropy becomes stronger in structures with thick CMS.

Fig. 2(b) shows R_{yx} as a function of $\mu_0 H_z$ for MnGa/CMS bilayers with various t_{CMS} ranging from 0 to 1.0 nm. The R_{yx} and the MOKE signals show similar hysteresis loops. Slight differences in coercive field between R_{yx} and MOKE signals are probably due to the influence of Hall-bar processing and/or Joule heating by current used for measurement of R_{yx}. Since MOKE signals reflect magnetization of MnGa for MnGa/CMS bilayers with t_{CMS} = 0 – 1.0 nm from magnetization measurement, R_{yx} for the MnGa/CMS bilayer is dominated by the anomalous Hall signal arising from the MnGa, and the magnetization direction of MnGa is detected from the values of R_{yx}.

B. SOT-induced effective magnetic field

We evaluated the effective magnetic field H_{eff} induced by the SOT acting on the magnetization in domain walls (DWs) created during magnetization reversal to clarify the SOT efficiency in the antiferromagnetically coupled MnGa/CMS bilayer [31]. To do this, we measured the shift of R_{yx}–$\mu_0 H_z$ curves under in-plane magnetic field H_x along current direction. Fig. 3(a) shows normalized R_{yx} as a function of $\mu_0 H_z$ under $\mu_0 H_x$ = ±300 mT and dc current I = ±12 mA for the device with t_{CMS} = 0.6 nm. When I and H_x are parallel (antiparallel), the center of the hysteresis loop was shifted in the negative (positive) H_z direction. These results can be explained as follows. The magnetization **m** in MnGa/CMS bilayer feels the effective field along $\mathbf{m} \times \mathbf{s_y}$ direction due to the spin current generated from the spin Hall effect in Ta, where $\mathbf{s_y}$ is electron spin which points along y-axis direction. When **m** in the DWs points along x–axis direction by H_x application, the effective field along z–axis direction is generated, which assists or hinders the DW motion, resulting in the shift of hysteresis loop. Thus, the shift amount of the hysteresis loop with respect to the center position corresponds to $\mu_0 H_{eff}$ acting on DWs. As shown in Fig. 3(b), the value of $\mu_0 H_{eff}$ increased almost linearly with increasing $|\mu_0 H_x|$ and saturated at large $|\mu_0 H_x|$. This saturation is due to the magnetization in the DWs being magnetized in the x-axis direction by sufficient $\mu_0 H_x$.

We carried out similar measurement on the devices with t_{CMS} ranging from 0 to 1.0 nm and obtained saturated values of $\mu_0 H_{eff}$. We divided the saturated value $\mu_0 H_{eff}^*$ by current density in Ta (J_{Ta}), which is a measure of SOT efficiency, and plotted them as a function of t_{CMS} in Fig. 4(a). Interestingly a significant increase of $\mu_0 H_{eff}^*/J_{Ta}$ was observed near the compensation point, and it took the maximum in the device with t_{CMS} = 0.6 nm, which is approximately 6 times as large compared with that in the device with t_{CMS} = 0.

Now we will discuss the origin of the variation of $\mu_0 H_{eff}^*/J_{Ta}$ with respect to t_{CMS}. According to the macro-spin model, the value of $\mu_0 H_{eff}^*/J_{Ta}$ is given by [9]

$$\left| \frac{\mu_0 H_{eff}^*}{J_{Ta}} \right| = \frac{\pi}{2} \frac{\hbar \theta_{SH}}{2 e m_s}, \quad (1)$$

where $\hbar$ is the Dirac constant, e is the elementary charge, θ_{SH} is the effective spin Hall angle, and m_s is the saturation magnetic moment per area. Fig. 4(b) and (c) show m_s and θ_{SH} as a function of t_{CMS}. The values of m_s were calculated from the relation given by

$$m_s = |M_s^{(MnGa)} \cdot t_{MnGa} - M_s^{(CMS)} \cdot t_{CMS}|, \quad (2)$$

where t_{MnGa} (= 2.5 nm) is the thickness of MnGa, $M_s^{(MnGa)}$ (≈ 1.6 × 10^5 A/m) and $M_s^{(CMS)}$ (≈ 8.0 × 10^5 A/m) are the saturation magnetization of MnGa and CMS, respectively, whose values were obtained by measuring the magnetization of a 2-nm-thick MnGa single layer and a MnGa(2)/CMS(1) bilayer fabricated under the same growth conditions [29]. Substituting m_s and $\mu_0 H_{eff}^*/J_{Ta}$ values into (1), we calculated θ_{SH} for each t_{CMS}. The m_s was modulated by approximately 10 times at $0 \leq t_{CMS} \leq 1$ nm, whereas the θ_{SH} is modulated by approximately 4 times. Therefore, the value of $\mu_0 H_{eff}^*/J_{Ta}$ depends more dominantly on the change of m_s than that of θ_{SH}.

Finally, we will discuss on the origin of the variation of θ_{SH} with respect to t_{CMS}. We obtained θ_{SH} = 0.009 at t_{CMS} = 0 [*see* Fig. 4(c)]. This value is smaller than the previously reported values for the Ta layer (0.12 - 0.15 [3]). This is possibly because the MnGa is relatively thick, in which case the SOT becomes

weak as the distance from the Ta/MnGa interface increases. Another reason is the influence of the spin current from NiAl layer. To confirm this, we measured the effective field for a 2.5-nm-thick MnGa single layer without Ta and obtained $\theta_{SH} \approx 0.001$ (*not shown*). This indicates that the NiAl buffer also generates weak spin current. Since the sign of θ_{SH} for Ta and that for NiAl is the same, the SOT induced by Ta and that by NiAl competes each other, resulting in the reduction of effective θ_{SH}. The θ_{SH} further decreased with increasing t_{CMS} from 0 to 0.42 nm because the insertion of CMS further reduces the SOT acting on the MnGa, which dominates total magnetic moment of the MnGa/CMS bilayer. However, the θ_{SH} increased rapidly up to 0.02 near the compensation point. This variation can be due to the inversion of the magnetization configuration before and after the compensation point, where total magnetic moment in MnGa (CMS) is dominant in MnGa/CMS bilayer with $t_{CMS} < 0.45$ nm (> 0.45 nm) [*see* Fig. 2(a)]. After the compensation point ($t_{CMS} > 0.45$ nm) the SOT from Ta acting on the CMS and that from NiAl acting on the MnGa cooperate to switch the MnGa/CMS, resulting in the increase of effective θ_{SH}. However, more exact models beyond the macro-spin model are necessary to fully understand the physical origins of complicated feature for t_{CMS}-dependence of θ_{SH}.

IV. Conclusion

We investigated the SOT-induced effective magnetic field in a structure consisting of Ta heavy metal layer and an antiferromagnetically coupled MnGa/CMS bilayer around the magnetization compensation point and found that the strength of the effective magnetic field was enhanced near the magnetization-compensation point mainly because of the reduction of total magnetic moment of MnGa/CMS. These results contribute to understanding of SOT in antiferromagnetically coupled bilayers and suggest the potential of realizing efficient SOT magnetization switching.

Acknowledgment

The authors thank T. Nagahama for the support with the MOKE measurement. This work was supported in part by the Japan Society for the Promotion of Science KAKENHI under Grants Nos. 20H02174 and 20H02598, and the Center for Spintronics Research Network.

References

[1] I. M. Miron, G. Gaudin, S. Auffret, B. Rodmacq, A. Schuhl, S. Pizzini, J. Vogel, and P. Gambardella, "Current-driven spin torque induced by the Rashba effect in a ferromagnetic metal layer," *Nat. Mater.*, vol. 9, pp. 230-234, Jan. 2010.

[2] I. M. Miron, K. Garello, G. Gaudin, P. -J. Zermatten, M. V. Costache, S. Auffret, S. Bandiera, B. Rodmacq, A. Schuhl, and P. Gambardella, "Perpendicular switching of a single ferromagnetic layer induced by in-plane current injection," *Nature*, vol. 476, pp. 189-193, Aug. 2011.

[3] L. Liu, C.-F. Pai, Y. Li, H. W. Tseng, D. C. Ralph, and R. A. Buhrman, "Spin-Torque Switching with the Giant Spin Hall Effect of Tantalum," *Science*, vol. 336, pp. 555-558, May 2012.

[4] L. Liu, O. J. Lee, T. J. Gudmundsen, D. C. Ralph, and R. A. Buhrman, "Current-Induced Switching of Perpendicularly Magnetized Magnetic Layers Using Spin Torque from the Spin Hall Effect," *Phys. Rev. Lett.*, vol. 109, 096602(5pp), Aug. 2012.

[5] C. -F. Pai, L. Liu, Y. Li, H. W. Tseng, D. C. Ralph, and R. A. Buhrman, "Spin transfer torque devices utilizing the giant spin Hall effect of tungsten," *Appl. Phys. Lett.*, vol. 101, 122404(4pp), Sep. 2012.

[6] M. Yamanouchi, L. Chen, J. Kim, M. Hayashi, H. Sato, S. Fukami, S. Ikeda, F. Matsukura, and H. Ohno, "Three terminal magnetic tunnel junction utilizing the spin Hall effect of iridium-doped copper," *Appl. Phys. Lett.*, vol. 102, 212408(4pp), May 2013.

[7] M. Cubukcu, O. Boulle, M. Drouard, K. Garello, C. O. Avci, I. M. Miron, J. Langer, B. Ocker, and P. Gambardella, "Spin-orbit torque magnetization switching of a three-terminal perpendicular magnetic tunnel junction," *Appl. Phys. Lett.*, vol. 104, 042406(5pp), Jan. 2014.

[8] S. Fukami, T. Anekawa, C. Zhang and H. Ohno, "A spin–orbit torque switching scheme with collinear magnetic easy axis and current configuration," *nature nanotech*, vol. 11, pp. 621-625, Jul. 2016.

[9] A. Thiaville, S. Rohart, E. Jue, V. Cros, and A. Fert, "Dynamics of Dzyaloshinskii domain walls in ultrathin magnetic films," *Eur. Phys. Lett.*, vol. 100, 57002(6pp), Dec. 2012.

[10] R. Ranjbar, K. Suzuki, A. Sugihara, Q. L. Ma, X. M. Zhang, T. Miyazaki, Y. Ando, and S. Mizukami, "Antiferromagnetic coupling in perpendicularly magnetized cubic and tetragonal Heusler bilayers," *Mater. Lett.*, vol. 160, pp. 88-91, Jul. 2015.

[11] M. Tanaka, J. P. Harbison, J. DeBoeck, T. Sands, B. Philips, T. L. Cheeks, and V. G. Keramidas, "Epitaxial growth of ferromagnetic ultrathin MnGa films with perpendicular magnetization on GaAs," *Appl. Phys. Lett.*, vol. 62, pp. 1565-1567, Jan. 1993.

[12] F. Wu, S. Mizukami, D. Watanabe, H. Naganuma, M. Oogane, Y. Ando, and T. Miyazaki, "Epitaxial $Mn_{2.5}Ga$ thin films with giant perpendicular magnetic anisotropy for spintronic devices," *Appl. Phys. Lett.*, vol. 94, 122503(3pp), Mar. 2009.

[13] L, J. Zhu, D. Pan, S. H. Nie, J. Lu, and J. H. Zhao, "Tailoring magnetism of multifunctional Mn_xGa films with giant perpendicular anisotropy," *Appl. Phys. Lett.*, vol. 102, 132403(5pp), Apr. 2013.

[14] T. Kubota, M. Araidai, S. Mizukami, X. Zhang, Q. Ma, H. Naganuma, M. Oogane, Y. Ando, M. Tsukada, and T. Miyazaki, "Composition dependence of magnetoresistance effect and its annealing endurance in tunnel junctions having Mn-Ga electrode with high perpendicular magnetic anisotropy," *Appl. Phys. Lett.*, vol. 99, 192509(3pp), Nov. 2011.

[15] R. Ranjbar, K. Z. Suzuki, Y. Sasaki, L. Bainsla, and S. Mizukami, "Current-induced spin–orbit torque magnetization switching in a MnGa/Pt film with a perpendicular magnetic anisotropy," *Jpn. J. Appl. Phys.*, vol. 55, 120302(4pp), Nov. 2016.

[16] K. Meng, J. Miao, X. Xu, Y. Wu, J. Xiao, J. Zhao, and Y. Jiang, "Modulated switching current density and spin-orbit torques in MnGa/Ta films with inserting ferromagnetic layers," *Sci. Rep.*, vol. 6, 38375(8pp), Dec. 2016.

[17] N. H. D. Khang, Y. Ueda, and P. N. Hai, "A conductive topological insulator with large spin Hall effect for ultralow power spin–orbit torque switching," *Nat. Mater.*, vol. 17, pp. 808-813, Sep. 2018.

[18] M. Yamanouchi, N. V. Bao, M. Inoue, and T. Uemura, "Interaction between spin-orbit torque and domain walls in a Ta/MnGa/NiAl structure," *Jpn. J. Appl. Phys.*, vol. 58, 100903(4pp), Sep. 2019.

[19] M. Takikawa, K. Z. Suzuki, R. Ranjbar, and S. Mizukami, "In-plane current-induced magnetization switching in CoGa/MnGa/MgO films," *Appl. Phys. Exp.*, vol. 10, 073004(4pp), Jun. 2017.

[20] M. Yamanouchi, N. V. Bao, F. Shimohashi, K, Jono, M. Inoue, and T. Uemura, "Magnetic properties and spin-orbit-torque-induced magnetization switching in Ta/MnGa grown on Cr and NiAl buffer layers," *AIP Advances*, vol. 9, 125245(4pp), Dec. 2019.

[21] M. P. Raphael, B. Ravel, Q. Huang, M. A. Willard, S. F. Cheng, B. N. Das, R. M. Stroud, K. M. Bussmann, J. H. Claassen, and V. G. Harris, "Presence of antisite disorder and its characterization in the predicted half-metal Co_2MnSi," *Phys. Rev. B*, vol. 66, 104429(6pp), Sep. 2002.

[22] S. Picozzi, A. Continenza, and A. J. Freeman, "Co_2MnX (X=Si, Ge, Sn) Heusler compounds: An *ab initio* study of their structural, electronic, and magnetic properties at zero and elevated pressure," *Phys. Rev. B*, vol. 66, 094421(9pp), Sep. 2002.

[23] I. Galanakis, P.H. Dederichs, and N. Papanikolaou, "Origin and properties of the gap in the half-ferromagnetic Heusler alloys," *Phys. Rev. B*, vol. 66, 134428(10pp), Oct. 2002.

[24] Y. Sakuraba, M. Hattori, M. Oogane, Y. Ando, H. Kato, A. Sakuma, and T. Miyazaki, "Giant tunneling magnetoresistance in Co_2MnSi/Al–O/Co_2MnSi magnetic tunnel junctions," *Appl. Phys. Lett.*, vol. 88, 192508, May 2006.

[25] T. Ishikawa, S. Hakamata, K. Matsuda, T. Uemura, and M. Yamamoto, "Fabrication of fully epitaxial Co_2MnSi/MgO/Co_2MnSi magnetic tunnel junctions," *J. Appl. Phys.*, vol. 103, 07A919(3pp), Apr. 2008.
[26] S. Tsunegi, Y. Sakuraba, M. Oogane, K. Takanashi, and Y. Ando, "Large tunnel magnetoresistance in magnetic tunnel junctions using a Co_2MnSi Heusler alloy electrode and a MgO barrier," *Appl. Phys. Lett.*, vol. 93, 112506(3pp), Sep. 2008.
[27] T. Ishikawa, H. Liu, T. Taira, K. Matsuda, T. Uemura, and M. Yamamoto, "Influence of film composition in Co_2MnSi electrodes on tunnel magnetoresistance characteristics of Co_2MnSi/MgO/Co_2MnSi magnetic tunnel junctions" *Appl. Phys. Lett.*, vol. 95, 232512(3pp), Dec. 2009.
[28] H. Liu, Y. Honda, T. Taira, K. Matsuda, M. Arita, T. Uemura, and M. Yamamoto, "Giant tunneling magnetoresistance in epitaxial Co_2MnSi/MgO/Co_2MnSi magnetic tunnel junctions by half-metallicity of Co_2MnSi and coherent tunneling," *Appl. Phys. Lett.*, vol. 101, 132418(5pp), Sep. 2012.
[29] K. Jono, F. Shimohashi, M. Yamanouchi, and T. Uemura, "Spin–orbit torque induced magnetization switching for an ultrathin MnGa/Co_2MnSi bilayer," *AIP Advances*, vol. 11, 025205(5pp), Feb. 2021.
[30] S. Li, J. Lu, S.-W. Mao, D.-H. Wei, and J.-H. Zhao, "Magnetic characterization of a thin Co_2MnSi/$L1_0$–MnGa synthetic antiferromagnetic bilayer prepared by MBE," *Chinese Phys. B*, vol. 29, 107501, Feb. 2020.
[31] C.-F. Pai, M. Mann, A.J. Tan, and G. S. D. Beach, "Determination of spin torque efficiencies in heterostructures with perpendicular magnetic anisotropy," *Phys. Rev. B*, vol. 93, 144409(7pp), Apr. 2016.

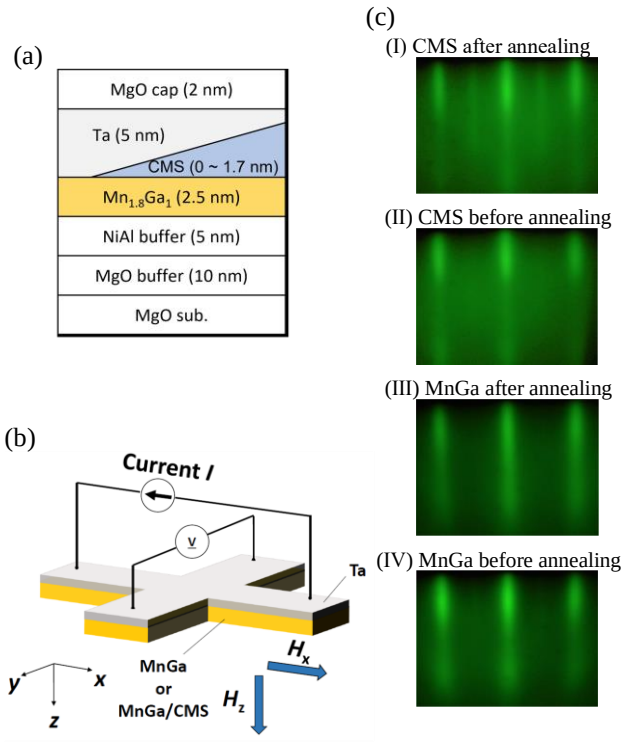

Fig. 1. Schematics of (a) a layer structure and (b) a typical Hall device with a 5-μm-wide channel with a definition of the Cartesian coordinate system. The transverse resistance R_{yx} was measured with an in-plane dc current I under application of in-plane magnetic field (H_x) and out-of-plane magnetic fields (H_z). (c) (Ⅰ) - (Ⅳ) RHEED patterns of MnGa and CMS before and after annealing. The electron beam azimuth was along MgO[100] direction. Clear streak patterns indicate the epitaxial growth of both MnGa and CMS.

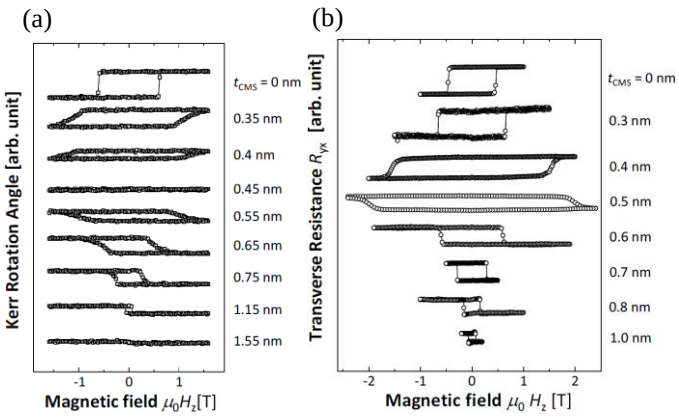

Fig. 2. (a) MOKE signals and (b) transverse resistance R_{yx} as a function of $\mu_0 H_z$ for MnGa/CMS bilayers with various t_{CMS}. The MnGa and CMS are antiferromagnetically coupled to each other with clear PMA at t_{CMS} < 1.55 nm. The magnetization compensation was realized at $t_{CMS} \approx 0.45$ nm.

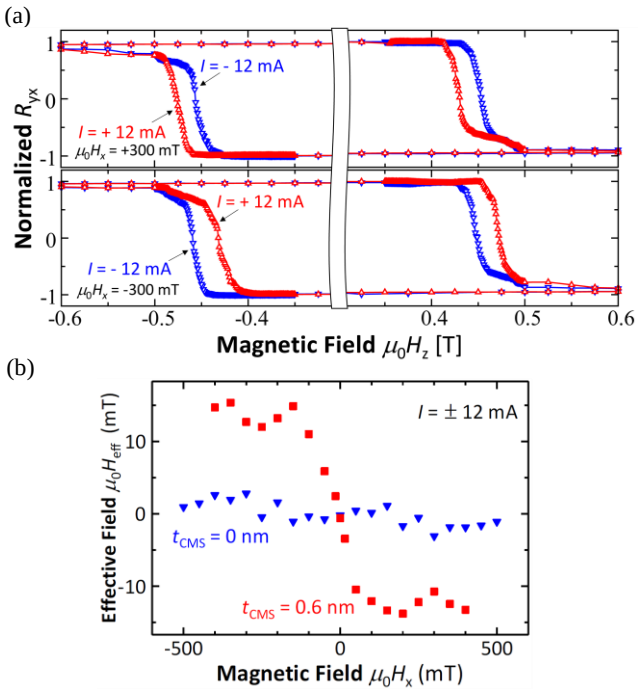

Fig. 3. (a) Normalized R_{yx} measured with I = ±12 mA as a function of $\mu_0 H_z$ under $\mu_0 H_x$ = ±300 mT for a device with t_{CMS} = 0.6 nm. The difference of coercive fields between R_{yx} - $\mu_0 H_z$ loop with positive I and that with negative I corresponds to $2\mu_0 H_{eff}$. (b) $\mu_0 H_{eff}$ as a function $\mu_0 H_x$ for the devices with t_{CMS} = 0 and 0.6 nm. Approximately 6-times as large H_{eff} was observed in the device with t_{CMS} = 0.6 nm compared with that in the device with t_{CMS} = 0.

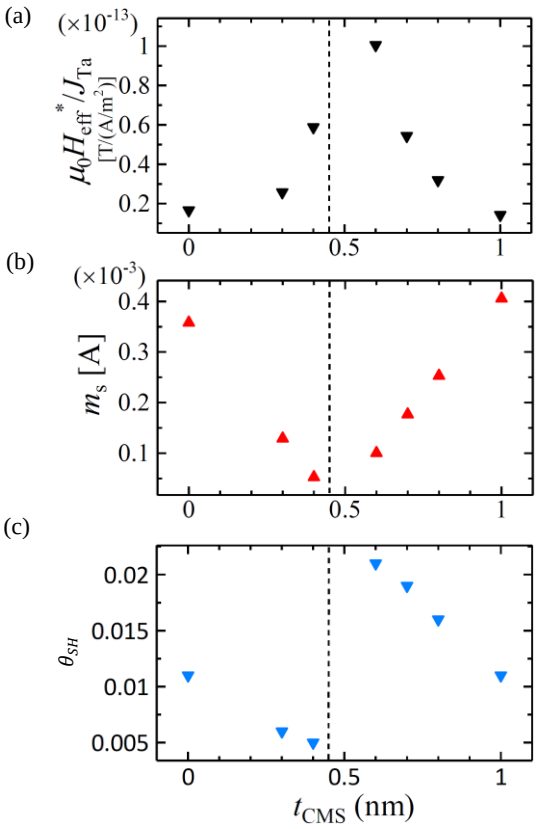

Fig. 4. (a) SOT efficiency $\mu_0 H_{\mathrm{eff}}^{*}/J_{\mathrm{Ta}}$, (b) calculated saturation magnetic moment m_{s}, and (c) effective spin Hall angle θ_{SH} calculated from (1), as a function of t_{CMS}. The black dotted line in each figure indicates the magnetization compensation point.